ISSN 1063-7710, Acoustical Physics, 2019, Vol. 65, No. 5, pp. 583–592. © Pleiades Publishing, Ltd., 2019.

ATMOSPHERIC AND AEROACOUSTICS

Study on Ground Vibration Mode of Physical Explosion of High Pressure Natural Gas Pipeline

Huayuan Ma[a], *, Yuan Long[a], **, Mingshou Zhong[a], *, Xinghua Li[a], ****, Quanmin Xie[a], *****, and Xingbo Xie [a], ******

[a]*Army Engineering University of PLA, Zhengzhou, China*

**e-mail: 503812350@qq.com*

***e-mail: long_yuan@sohu.com*

****e-mail: zhongms7@126.com*

*****e-mail: bifs@qq.com*

******e-mail: 13797006996@163.com*

*******e-mail: znbxie@126.com*

Received October 12, 2018; revised January 9, 2019; accepted May 7, 2019

Abstract—In this paper, an explosion experiment was carried out on the OD1219mm-X90-12Mpa natural gas pipeline to study the vibration hazard. Based on a series of experiments, the spatial distribution of the vibration energy was studied. The vibration distribution field was drawn by interpolation method based on re-harmonic equation and it was found that the field was non-circular symmetry. Through in-depth research, it was preliminarily proved that the vibration field had interference characteristics, which was caused by the special vibration source of the pipeline explosion. There was a significant difference in the frequency components between the interference strengthened region and the weakened region. The results shown that the strengthening effect of the interference in the 90° and 30° direction should be taken into account when evaluating the damage scope of the explosion accident. Research provided reference for safety design of parallel pipelines and buildings.

Keywords: natural gas pipeline, explosion vibration, spatial distribution, spectrum analysis, interference effect, time-frequency characteristic

DOI: 10.1134/S1063771019050142

INTRODUCTION

Due to environmental corrosion, material failure, natural disasters and other unknown factors, pipeline accidents happened frequently, which lead to a large number of casualties and collapse of the surrounding buildings [1, 2] as shown in Fig. 1. Therefore, it was necessary to study the hazards of natural gas pipeline explosion.

At present, the research on the hazards of natural gas pipeline explosion was mainly about thermal effect and flame hazard [3–6]. Most studies on vibration were limited to numerical simulations. Mishra K. B. [7] investigated scenarios of underground gas pipeline failure, crater formation, dispersion of gas, explosion and subsequent fires with semi-empirical and with CFD (Computational Fluid Dynamics) modelling. This research demonstrated a strong capability of CFD to assess the pre or/and post events foresee abilities within a reasonable amount of time and with an acceptable level of accuracy meeting the industrial needs for risk analysis. Su Hua-you [8] studied the dynamic response of underground pipeline under compound vibration loading mode by establishing a nonlinear mathematical model of soil-pipe coupling effect. The influence of vibration on the pipeline was analyzed, and the method is obtained to evaluate the seismic performance of buried pipeline. Mahdavi H. [9] studied the load transfer characteristics of underground pipelines in cohesive soils. The geometrical effects of pipe backfill and channel width was analyzed, and there are obtained soil strength distribution and response factors.

In summary, there was a lack of research on vibration wave of pipeline explosion. The research results of this paper provided theoretical and technical support for comprehensively understanding the hazard effect of natural gas pipeline explosion.

Fig. 1. Case of pipeline explosion. (a) New Mexico, 2000; (b) Ukraine, 2007; (c) Shenzhen, China, 2015.

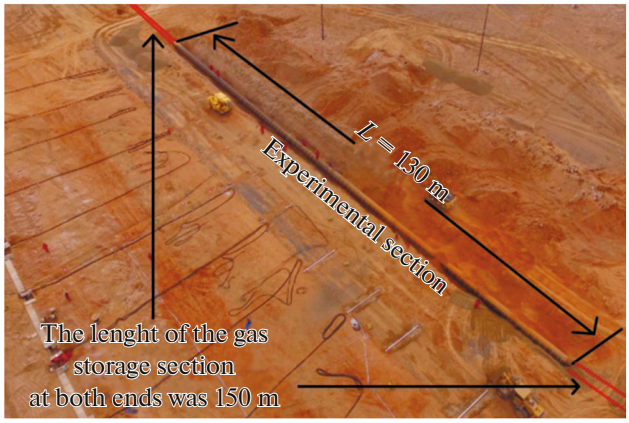

Fig. 2. Aerial image of the experimental pipeline.

1. EXPERIMENT OF OD1219-X90-12MPA PIPELINE EXPLOSION

1.1. Scheme of the Experiment

The experiment selected the third-generation natural gas pipeline. This type of pipeline had been widely used in the West-East Gas Pipeline Project [10, 11]. Parameters were shown in Table 1. The total length of the experimental pipeline was 430 m, and it had two sections. The length of the gas storage section at both ends was 150 m, and the length of the experimental section in the middle of the pipeline was 130 m, as shown in Fig. 2. Pipeline was filled with natural gas, and the inner pressure was 12 Mpa. The gas components were shown in Table 2.

In order to make the pipeline explode, a linear shaped charge cutter with length of 500 mm was set along the axis in the middle of the experimental section to introduce the initial crack, as shown in Fig. 3. The gas storage components were first buried. After the preparation was completed, the experimental part was subsequently buried. In order to simulate the worst case after a pipe explosion, the ignition device was set to ignite the leaked natural gas.

Took the initiation point as the coordinate origin, the measurement lines were set in 4 directions. The measurement line L1 was 90° angle to the pipeline, L2 was 60°, L3 was 30°, and L4 was 0°. At each measurement point, a vibration velocity sensor and a vibration acceleration sensor were placed. The distribution of the measurement points was shown in Fig. 4. In order to solve the coupling problem between sensors and natural gravel soil, the authors designed a special sensor installation platform, as shown in Fig. 5.

Vibration recorders used in the experiment were type TC-4850 and type Blast-UM. The two types of recorders were equipped with three-vector sensors, which could record three mutually perpendicular (X-axis, Y-axis, Z-axis) vibration. Parameters were shown in Table 3. Before the experiment, all the recorders and sensors were calibrated in Jiangsu Metrology Institute to ensure the authenticity of the data. The trigger threshold was set to 0.1 cm/s (vibration velocity recorders), 0.1 g (vibration acceleration recorders), the sampling frequency was set to 10000 Sps and the acquisition time was set to 10 s .

Table 1. Parameters of the experimental pipeline

Piping material	Diameter, mm	Modulus of elasticity, GPa	Poisson ratio	Yield strength, MPa	Wall thickness, mm	Buried depth, m	Pressure, MPa
X90	1219	206	0.3	716	16.3	1.2–1.3	12

Table 2. Composition of the experimental gas

Component	CH_4	CH_3CH_3	CO_2	N_2	Other gases
Mol %	94.91	2.55	0.94	1.4	0.2

1.2. Experiment Process and Phenomenon

When everything was ready, the first step was to fire the ignition bomb and then detonated the cutter. The pipe was penetrated by the jet to form an initial crack. It was broken and natural gas was sprayed. After come into contact with the ignition bomb, the leaked natural gas was ignited. The maximum diameter of the fireball was about 180 m, and the maximum height of the mushroom cloud was about 300 m, as shown in Fig. 6. At the first moment after the explosion, UAVs (unmanned aerial vehicle) were sent to conduct investigations on the explosion site. It could be seen that the explosion created a crater with a size of 17 × 7 m. Crack was extended by about 17 m, as shown in Fig. 7. The vibration data was shown in Table 4.

Previously, authors had successfully carried out two high-pressure natural gas pipeline explosion experiments. By analyzing the data, authors found that the vibration intensity was related to the angle between the measurement line and pipeline. Previous data overview as shown in Fig. 8. Therefore, this experiment aimed to study the spatial distribution of vibrations in natural gas pipeline explosions.

2. VIBRATION SPATIAL DISTRIBUTION

2.1. Experiment Data Analysis

Vibration data of different lines were shown in the Fig. 9. It could be seen from the figure that the vibration intensity exhibited a nonlinear characteristic with the attenuation of the distance. In the study of predecessors, the attenuation law of explosion vibration followed the power distribution [12, 13]. However, authors found that the vibration of pipeline explosion was more consistent with the exponential decay law, as shown in Fig. 10.

It could be seen that the result of exponential fitting had higher goodness of fit. Exponential fitting had smaller SSE (Sum of Squares due to Error), and its R-square was closer to 1. Therefore, in this paper, expo-

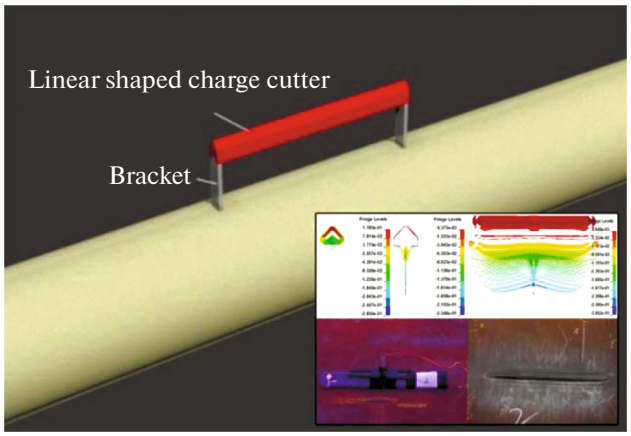

Fig. 3. Assembly diagram of the shaped charge cutter.

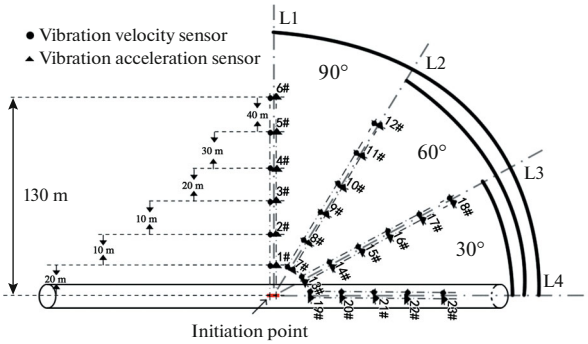

Fig. 4. Layout of measurement points.

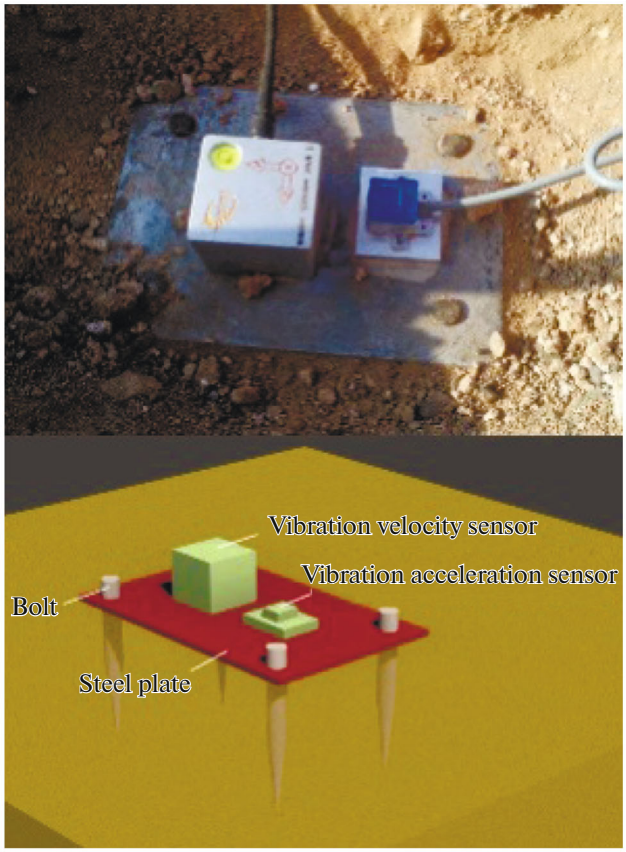

Fig. 5. Sensors assembly method.

Table 3. Technical parameters of the vibration recorders

Type	Sensor type	Number of the channels	Trigger Threshold	Resolution	Sampling Rate, Sps
Blast-UM	Acceleration Sensor	3	0.1 g	0.01 g	10 k
TC-4850	Velocity Sensor	3	0.1 cm/s	0.01 cm/s	10 k

Table 4. Vibration velocity data

Distance, m		20	30	40	60	90	130
Vibrating speed vector sum, cm/s	L1(90°)	1#	2#	3#	4#	5#	6#
		13.16	10.79	7.60	3.58	1.90	
	L2(60°)	7#	8#	9#	10#	11#	12#
		9.00	6.31	5.17	1.50	1.32	
	L3(30°)	13#	14#	15#	16#	17#	18#
		11.86	9.68	6.52	2.79	1.53	0.65
	L4(0°)	19#	20#	21#	22#	23#	
		9.33	7.34	4.22	1.16	0.54	

nential distribution was used to fit vibration data. The results were shown in the following forms.

$$\text{Measurement line } 90°: \quad V = 24.37e^{-0.029r}, \qquad (1)$$

$$\text{Measurement line } 60°: \quad V = 17.91e^{-0.034r}, \qquad (2)$$

$$\text{Measurement line } 30°: \quad V = 22.97e^{-0.031r}, \qquad (3)$$

$$\text{Measurement line } 0°: \quad V = 22.30e^{-0.041r}, \qquad (4)$$

where V was the vibration velocity, cm/s, r was the distance from the initiation point, m.

For a more vivid description, the tube axis was taken as the X-axis, and the vertical line of the pipe passing through the initiation point was taken as the Y-axis. A coordinate plane is constructed. Since the measurement points were mainly distributed in the first quadrant, authors performed two image expansions of the data and extended it to four quadrants. The spatial distribution of the vibration velocity was obtained by the method of spatial surface fitting based on Biharmonic spline interpolation [14, 15], as shown in Fig. 11.

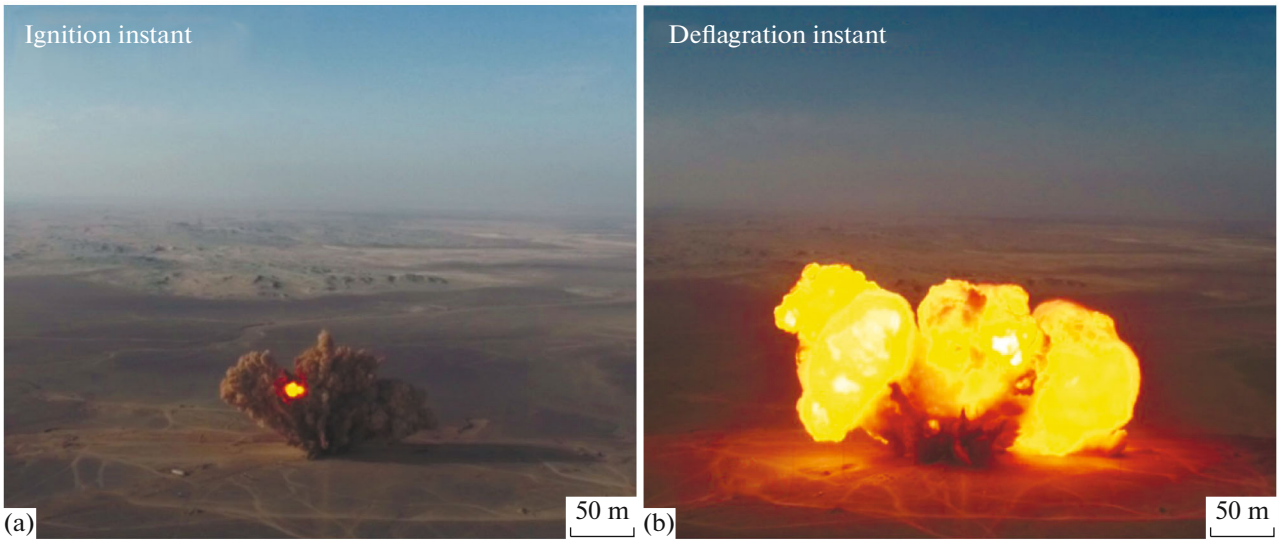

Fig. 6. Explosion process.

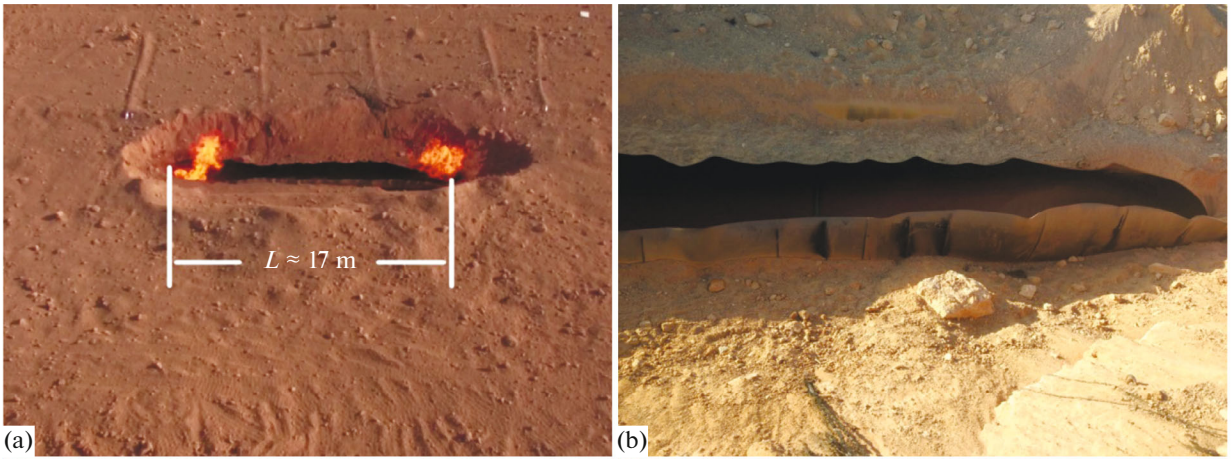

Fig. 7. Cracks in pipeline after the explosion.

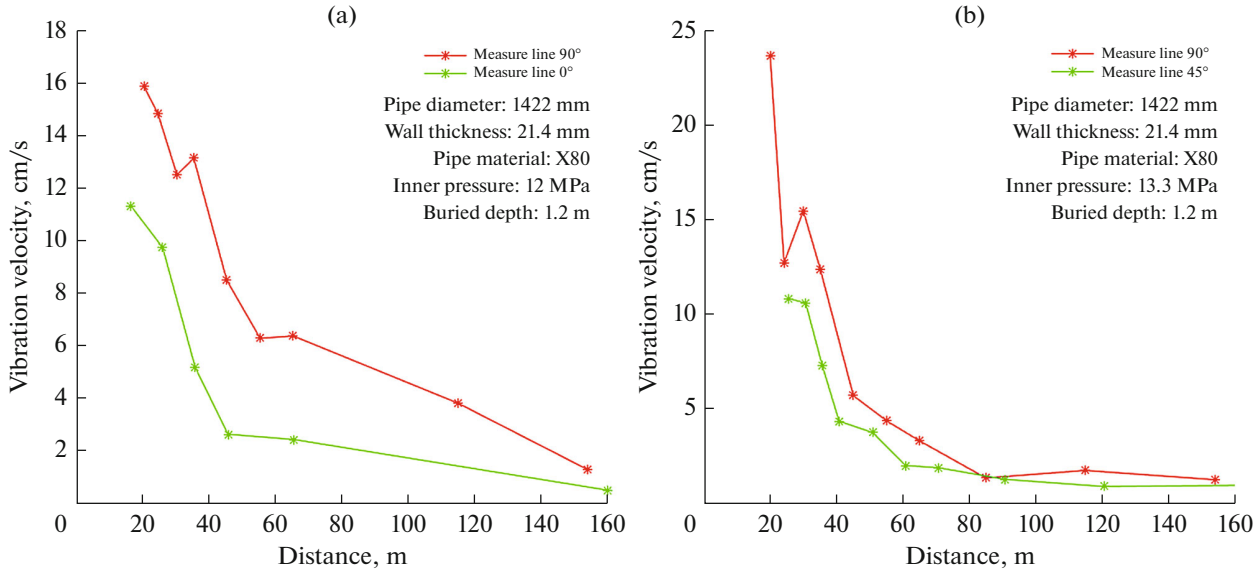

Fig. 8. Data overview of previous two experiments.

Z-axis represented the peak of vibration velocity. In the top view, it was obvious that the vibration field was snowflake-shaped with six lobes. Obviously, it was non-circularly symmetric. The vibration intensity was strengthened in certain regions, and weakened in others. This special vibration mode was different from a general explosion. Authors believed that it might be caused by the special vibration source of the pipeline explosion. The group-charge used in general explosion could be regarded as "point source", while the pipeline explosion was "linear source". That was possible to form an interference superposition of waves.

2.2. MATLAB Simulation

In order to verify the conjecture, MATLAB was used to build a simulation model. Set up a plane with 221 × 201 cells; origin coordinate was (111,101).

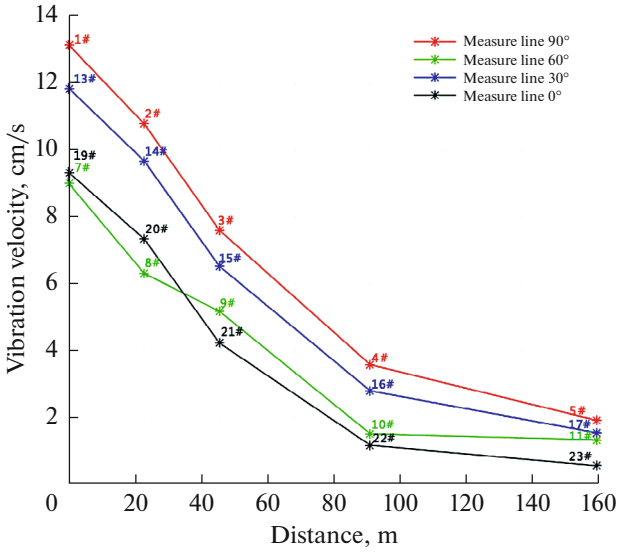

Fig. 9. Vibration data.

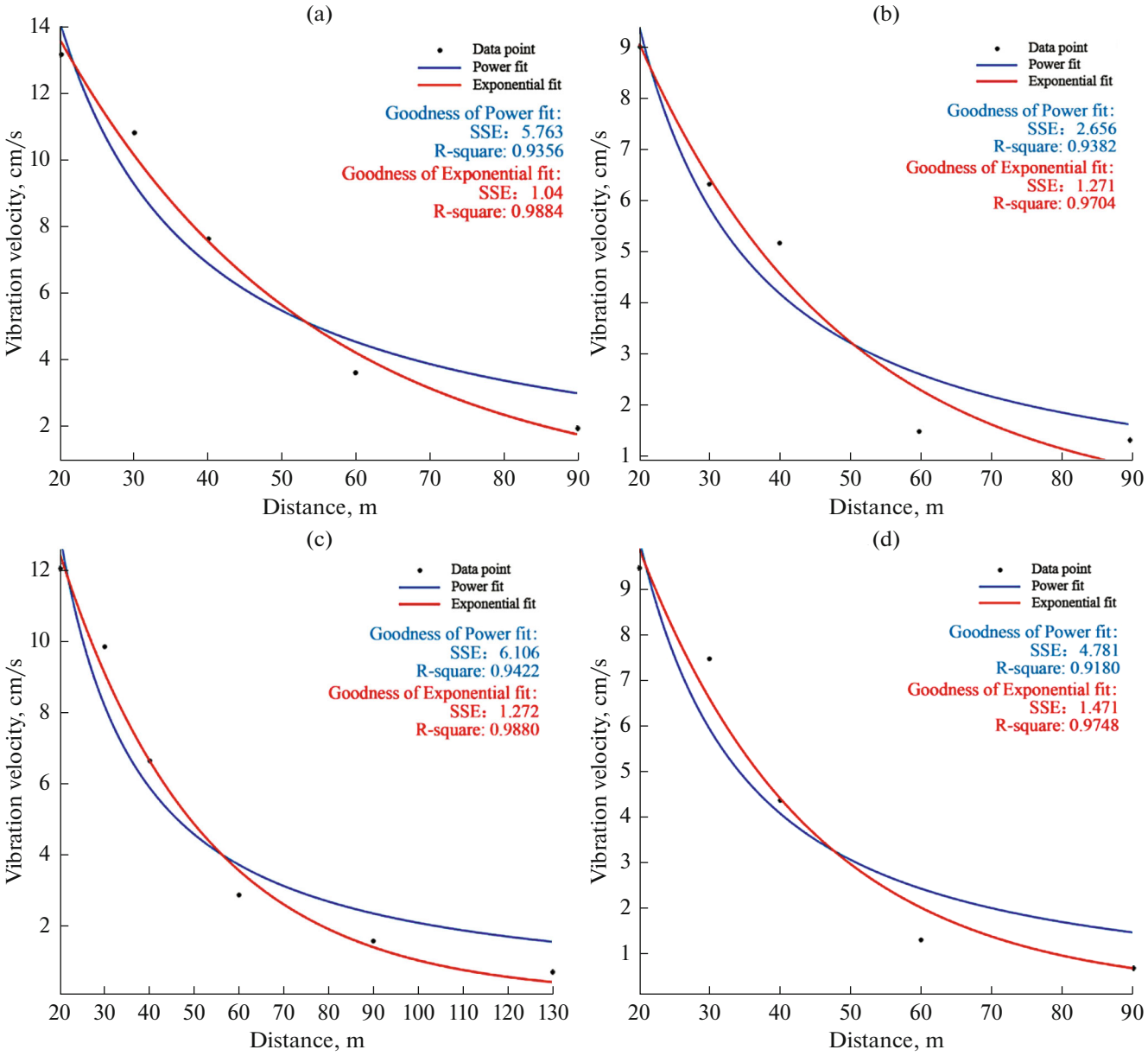

Fig. 10. Comparison of fitting effect. (a) 90° measurement line, (b) 60° measurement line, (c) 30° measurement line, (d) 0° measurement line.

According to the experiment data, the length of the crack was 17.43 m. So, took the (103.101)–(119.101) 17 points as the vibration source. The wave was simplified as sine wave, whose amplitude decreased exponentially with distance. It was known that interference was related to wavelength. Different interferogram were obtained by changing the wavelength in the simulation, as shown in Fig. 12.

It could be seen from the interferogram that the vibration intensity was strengthened in different directions as the wavelength changed. When the wavelength was set to 9–10 m, the simulated interferogram was similar to the experiment data. This result preliminarily proved that the asymmetric phenomenon observed from the experimental data might be caused by the interference effect. What's more, it also showed that wavelength of the wave that caused the interference in the experiment is about 9 to 10 meters.

Therefore, the strengthening effect of the interference in the vertical direction and the 30° direction should be taken into account when evaluating the damage scope of the explosion accident, as shown in Fig. 13. At the same time, engineers should consider increasing the safety distance in the vertical direction

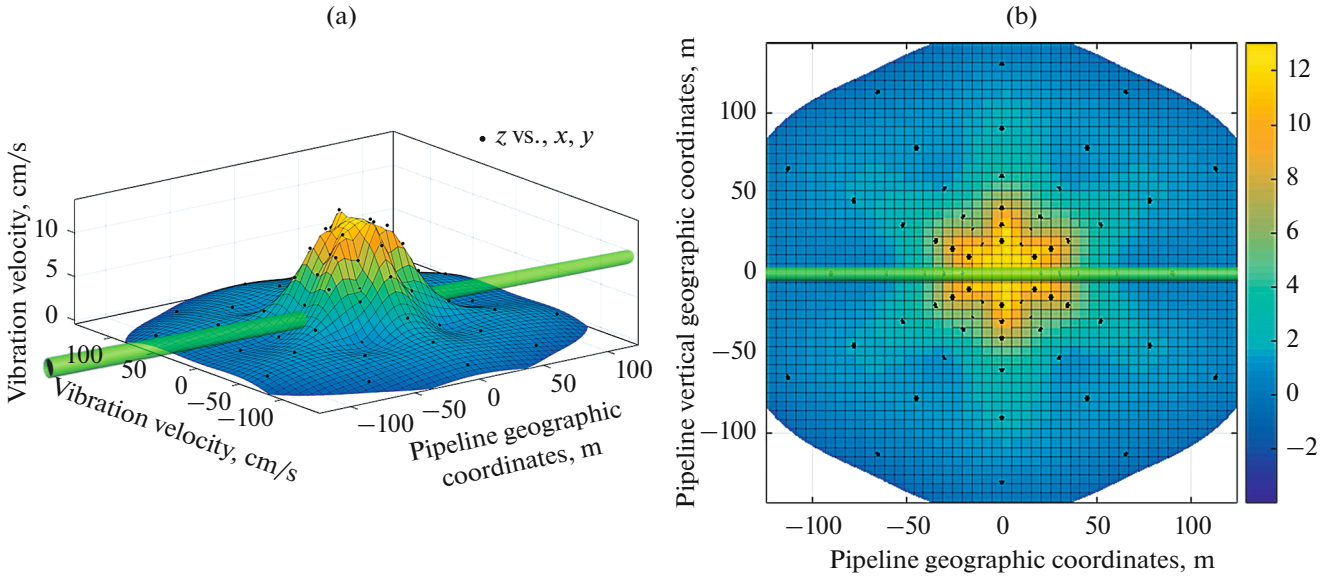

Fig. 11. The space distribution of the vibration velocity peak. (a) Perspective, (b) top view.

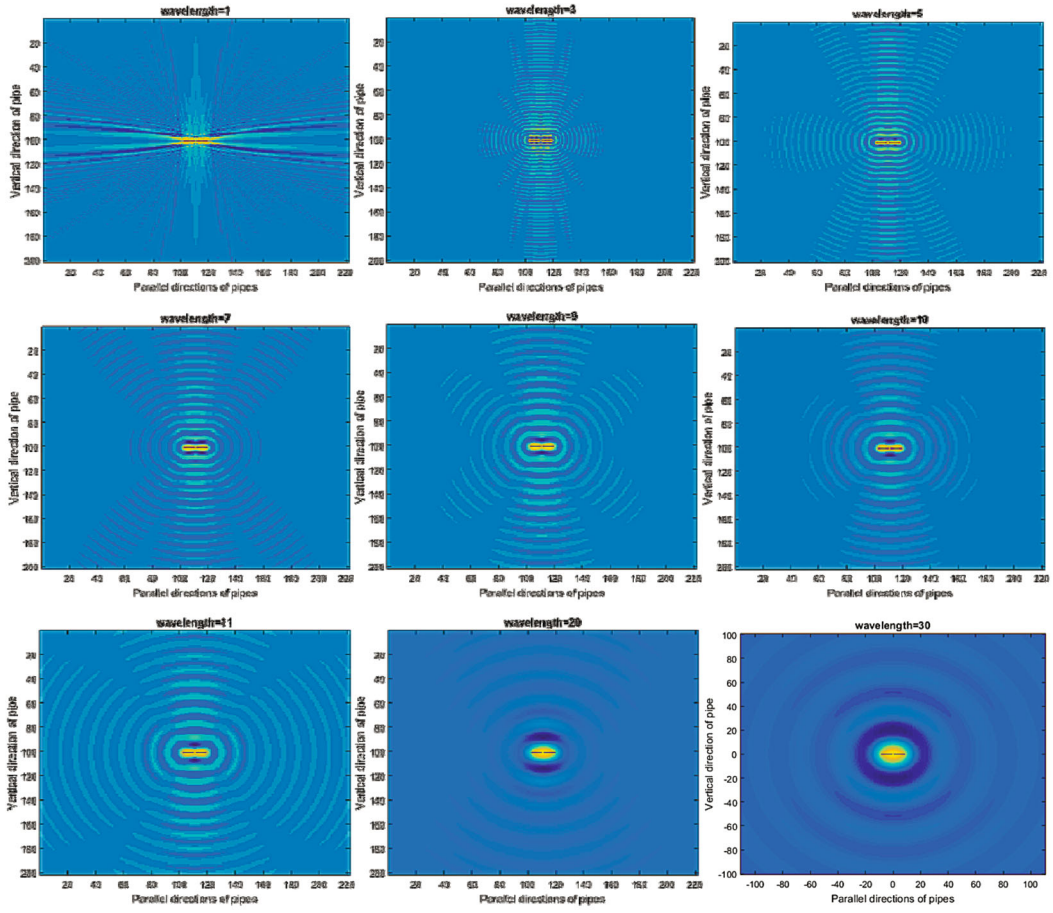

Fig. 12. Interferogram of different wavelengths.

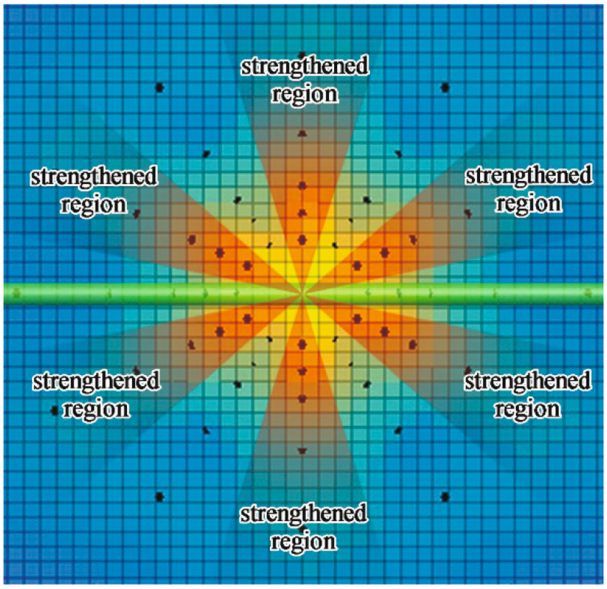

Fig. 13. The interference strengthened region.

and the 30° direction when doing safety design of the position with a high risk of leakage.

2.3. Time-Frequency Analysis of Vibration Signals

For further study, the time-frequency analysis method was adopted to compare the vibration in the strengthened and weakened regions. Pipeline explosion had multiple energy release processes, and they had a chronological order [16, 17]. Therefore, the HHT (Hilbert–Huang Transform) improved algorithm was introduced to analysis the signal in time-frequency domain.

Firstly, the signal $Z(t)$ was decomposed into multiple intrinsic modal functions $c(t)$ by EEMD (Ensemble Empirical Mode Decomposition) algorithm [18, 19]. Then, performed a Hilbert transformation on $c(t)$:

$$H[c(t)] = \frac{1}{\pi} PV \int_{-\infty}^{\infty} \frac{c(t')}{t - t'} dt', \tag{5}$$

where PV represented the Cauchy principal value. Establish analytic signal $Z(t)$:

$$z(t) = c(t) + jH[c(t)] = a(t) e^{j\Phi(T)}, \tag{6}$$

where $a(t)$ was the amplitude function and $\Phi(t)$ was the phase function.

$$a(t) = \sqrt{c^2(t) + H^2[c(t)]}, \tag{7}$$

$$\Phi(t) = \tan^{-1} \frac{H[c(t)]}{c(t)}. \tag{8}$$

The instantaneous amplitude and instantaneous phase of the wave could be obtained by differentiating the amplitude and phase. Further, the instantaneous frequency was obtained. After the Hilbert transform, the amplitude of the signal in the time-frequency domain could be obtained, known as the Hilbert spectrum. The expression was:

$$H(\omega, t) = \mathrm{Re} \sum_{i=1}^{n} a_i(t) e^{\int \omega_i(t) dt}. \tag{9}$$

The Hilbert spectrums of the measurement point 3# and 9# were obtained, as shown in Fig. 14.

As shown in the figure, the Hilbert energy loading processes of the two points were similar. The first wave that arrived, the frequency range was 0...100 Hz. After that, the peak arrived and the frequency range was

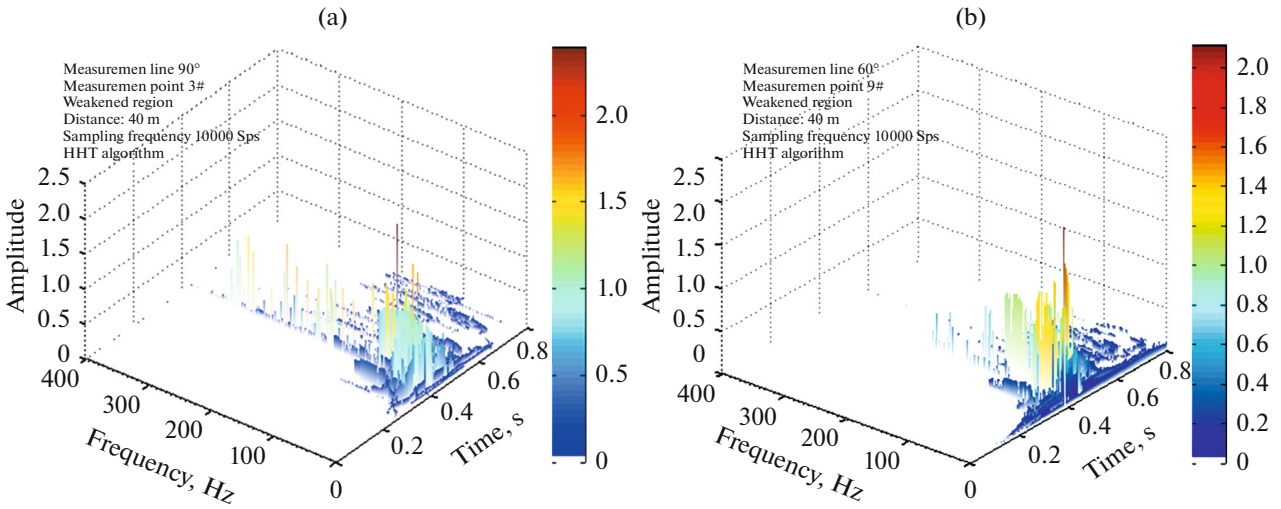

Fig. 14. Hilbert time-frequency spectrum of the measurement point 3# and 9# (Z-axis). (a)—measurement point 3#, (b)—measurement point 9#.

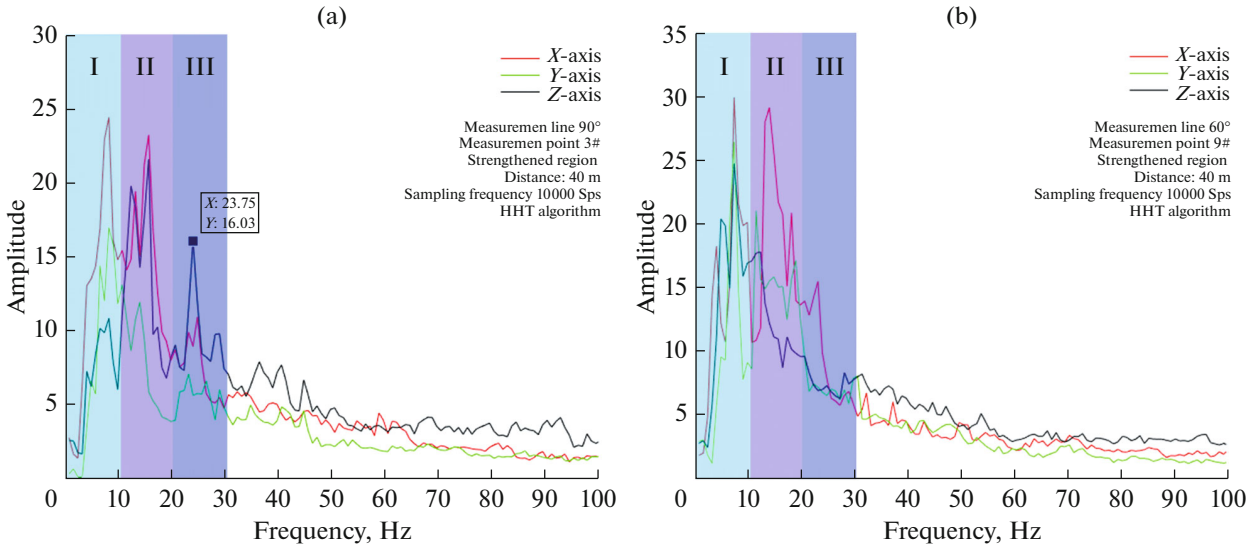

Fig. 15. Hilbert marginal spectrum. (a) Measurement point 3# (strengthened region), (b) measurement point 9# (weakened region).

wider, about 0...200 Hz. Finally, there was a low-frequency component with a longer duration. In the interference strengthened region, the frequency distribution was wider; there was still some energy distribution above 200 Hz. On the other hand, the low-frequency components of the interference weakened region last longer.

The marginal spectrum could be obtained by time integration of Hilbert spectrum; it presented the vibration components in the frequency domain, as shown in Fig. 15.

The vibration frequency of the *X*-axis and *Y*-axis signals of the two points were approximately similar. However, there was a significant difference in the distribution of *Z*-axis signals. It could be seen that the *Z*-axis signal in the strengthened region was mainly distributed in area II (10...20 Hz) and area III (20...30 Hz). While, the *Z*-axis signal in the weakened region was mainly distributed in area I (0...10 Hz). This difference indicated that it was highly probable that the frequency components in these two ranges caused interference effects. Each building actually has an infinite number of natural frequencies. From small to large, we call it the first frequency (base frequency) and the second frequency. The deformation state of the object corresponding to each natural frequency is called the vibration type. The main influences on the response of objects (such as displacement, internal force, etc.) are the first few low frequencies, while the higher order frequencies or modes have less effect on the response of objects. So that, the natural frequencies of buildings around pipelines, such as pressurized stations or parallel pipelines, should avoid this range of frequencies, especially in the interference strengthened region.

3. DISCUSSION

Through experiments and data analysis, the preliminary conclusions of the explosion vibration damage of OD1219mm-X90-12Mpa natural gas pipeline were obtained.

Compared with the power function, the attenuation of pipeline explosion vibration was more consistent with the exponential law. The vibration intensity distribution of pipeline explosion was related to the angle between the measurement line and the pipeline, but it was not monotonous. The vibration intensity was strengthened in certain regions, and weakened in others. Therefore, engineers should take the angle into consideration when doing safety design or damage assessment.

This directionality characteristic was caused by the interference of vibration. Moreover, the simulation results showed that the dominant wave length, which caused the interference, was about 9–10 m. The vibration frequency components were mainly distributed within the low frequency range of 0...100 Hz. There was a significant difference in the frequency components between the interference strengthened region and the weakened region.

Since the characteristics of the vibration generated by the explosion were related to the source of explosion and the soil medium, the results obtained in this experiment were applicable to the OD1219mm-X90 pipeline. At present, in the West-East Gas Pipeline

project, a considerable length of pipeline meet this applicable condition. For other specifications of pipelines or other soil media, there was still a lot of work needed to be supplemented by scholars.

FUNDING

This research was supported by the National Natural Science Foundation of China nos. 11672331 and 51608530. The authors would like to gratefully acknowledge this support.

DATA AVAILABILITY STATEMENT

The data used in this paper can be obtained in the following links.

https://figshare.com/s/e2aea8d0ff64d0fcebed

As the data laws continue to be studied, the data at other measurement points is not supported for download.

REFERENCES

1. Shuai Jian, J. Oil Gas Storage Transp. **29** (114), 806 (2010).
2. Hu Dengming and Luo Hui, J. Technol. Superv. Pet. Ind., No. 9, 8 (2009).
3. F. Y. Gao, C. Ji, Y. Long, and K. J. Song, Lat. Am. J. Solids Struct. **11** (11), 1924 (2014).
4. R. Eiber, T. Bubenik, and W. Maxey., *Fracture Control Technology for Natural Gas Pipelines,* A.G.A. NG-18 Report No. 208 (1993).
5. D. Baraldi, A. Kotchourko, A. Lelyakin, J. Yane, P. Middha, O. R. Hansen, and V. Molkov, Int. J. Hydrogen Energy **34** (18), 7862 (2009).
6. E. Gallego, E. Migoya, J. M. Martin-Valdepenas, A. Crespo, J. Garcia, A. Venetsanos, E. Papanikolaoub, S. Kumarc, E. Studerd, Y. Dagbae, T. Jordanf, W. Jahng, S. Høiseth, D. Makarovi, and J. Piechna, Int. J. Hydrogen Energy **32** (13), 2235 (2007).
7. K. B. Mishra and K. D. Wehrstedt, J. Nat. Gas Sci. Eng. **24**, 526 (2015).
8. Su Hua-you, Huang Jin, Xiao Ding-jun, and She Yanhua, Procedia Eng. **26**, 1835 (2011).
9. H. Mahdavi, S. Kenny, R. Phillips, and R. Popescu, in *Proc. 7th Int. Pipeline Conference, American Society of Mechanical Engineers* (Calgary, 2008), p. 543.
10. Zhang Zhenyong, Zhang Wenwei, Zhou Yawei, et al., Oil Gas Storage Transp. **36** (09), 1059 (2017). https://doi.org/10.6047/j.issn.1000-8241.2017.09.013
11. Huo Chunyong, Li He, Zhang Weiwei, et al., J. Nat. Gas Ind. **36** (06), 78 (2016). https://doi.org/10.3787/j.issn.1000-0976.2016.06.012
12. Li Hongtao, Lu Wenbo, Shu Daqiang, et al., Chin. J. Rock Mech. Eng. **29** (S1), 3364 (2010).
13. Lu Tao, Shi Yongqiang, Huang Cheng, et al., J. Rock Soil Mech., No. 09, 1871 (2007).
14. Gu Yanchun, Ma contends, and Liang Yutao, J. Zhongshan Univ. (Nat. Sci. Ed.), No. 05, 82–90 (2013).
15. Wang Yatao, Dong Lanfang, and Ni Kui, Chin. J. Image Graphics, No. **12**, 2189 (2007).
16. W. M. Telford, L. P. Geldart, and E. S. Robert, *Applied Geophysics* (Cambridge Univ. Press, Cambridge, 1990).
17. L. B. Freund, *Dynamic Fracture Mechanics* (Cambridge Univ. Press, Cambridge, 1998).
18. Chen Yangkang, Zhang Guoyin, Gan Shuwei, and Zhang Chenglin, J. Appl. Geophys. **119**, 99 (2015).
19. Chen Yangkang, Geophys. J. Int. **206**, 457 (2016).
20. B. N. Leis, S. M. Pimputkar, and N. D. Ghadiali, *Line Rupture and the Spacing of Parallel Lines, PRCI Report PR-003-9604* (American International Pipeline Research Council, 2002).
21. A. Lamis and A. Anders, J. Eng. Struct., No. 35, 11 (2012).
22. Z. Yan, A. Miyamoto, and Z. Jiang, J. Comput. Struct. **89** (1), 14 (2011).
23. X. Li, Y. Long, C. Ji, M. Zhong, and H. Zhao, J. Vibroeng. **15** (3), 1454 (2013).
24. S. Yang, Q. Fang, Y. Zhang, H. Wu, and L. Ma, J. Loss Prev. Process Ind. **26** (1), 74 (2013).
25. B. N. Leis, X. K. Zhu, and T. P. Forte, *in Proc. Pipeline Technology Conference* (Ostend, 2009), p. 12.
26. B. J. Lowesmith and G. Hankinson, Process Saf. Environ. Prot. **91** (1), 101 (2013).
27. Gang Dong, Lin Xue, Yun Yang, and Juntao Yang, J. Loss Prev. Process Ind. **23** (4), 522 (2010).
28. Spyros Sklavounos and Fotis Rigas, J. Loss Prev. Process Ind. **19** (1), 24 (2006).